Available online at www.sciencedirect.com
ScienceDirect
Journal of Computational Physics 227 (2007) 763–775
JOURNAL OF COMPUTATIONAL PHYSICS
www.elsevier.com/locate/jcp

A lattice Boltzmann method for incompressible two-phase flows on partial wetting surface with large density ratio

Y.Y. Yan *, Y.Q. Zu

School of the Built Environment, University of Nottingham, Nottingham NG7 2RD, UK

Received 7 December 2006; received in revised form 4 June 2007; accepted 22 August 2007
Available online 30 August 2007

Abstract

This paper reports a new numerical scheme of the lattice Boltzmann method for calculating liquid droplet behaviour on particle wetting surfaces typically for the system of liquid–gas of a large density ratio. The method combines the existing models of Inamuro et al. [T. Inamuro, T. Ogata, S. Tajima, N. Konishi, A lattice Boltzmann method for incompressible two-phase flows with large density differences, J. Comput. Phys. 198 (2004) 628–644] and Briant et al. [A.J. Briant, P. Papatzacos, J.M. Yeomans, Lattice Boltzmann simulations of contact line motion in a liquid–gas system, Philos. Trans. Roy. Soc. London A 360 (2002) 485–495; A.J. Briant, A.J. Wagner, J.M. Yeomans, Lattice Boltzmann simulations of contact line motion: I. Liquid–gas systems. Phys. Rev. E 69 (2004) 031602; A.J. Briant, J.M. Yeomans, Lattice Boltzmann simulations of contact line motion: II. Binary fluids, Phys. Rev. E 69 (2004) 031603] and has developed novel treatment for partial wetting boundaries which involve droplets spreading on a hydrophobic surface combined with the surface of relative low contact angles and strips of relative high contact angles. The interaction between the fluid–fluid interface and the partial wetting wall has been typically considered. Applying the current method, the dynamics of liquid drops on uniform and heterogeneous wetting walls are simulated numerically. The results of the simulation agree well with those of theoretical prediction and show that the present LBM can be used as a reliable way to study fluidic control on heterogeneous surfaces and other wetting related subjects.

Keywords: Lattice Boltzmann method (LBM); Two-phase flow; Large density ratio; Fluid droplet; Partial wetting; Contact angle

1. Introduction

In recent years, the LBM has become an established numerical scheme for simulating multi-phase fluid flows. The key idea behind the LBM is to recover correct macroscopic motion of fluid by incorporating the complicated physics of problem into a simplified microscopic models or mesoscopic kinetic equations. In this method, kinetic equations of particle velocity distribution function are first solved; macroscopic quantities are then obtained by evaluating hydrodynamic moments of the distribution function. This intrinsic feature

* Corresponding author. Tel.: +44 (0) 115 951 3168; fax: +44 (0) 115 951 3159.
E-mail address: yuying.yan@nottingham.ac.uk (Y.Y. Yan).

0021-9991/$ - see front matter © 2007 Elsevier Inc. All rights reserved.
doi:10.1016/j.jcp.2007.08.010

enables the LBM to model phase segregation and interfacial dynamics of multi-phase flow, which are difficult to be handled by applying conventional CFD methods or employing the molecular dynamics (MD) method to incorporate intermolecular interactions at mesoscopic level. The LBM has demonstrated a significant potential and broad applicability with many computational advantages including the parallel of algorithm and the simplicity of programming [5]. In order to simulate multi-phase fluid flows, Gunstensen et al. [6] developed a multi-component LBM on the basis of two-component lattice gas model. Shan and Chen [7] presented a LBM model with mean-field interactions for multi-phase and multi-component fluid flows. Later, Swift et al. [8,9] proposed a LBM model for multi-phase and multi-component flows using the idea of free energy; He et al. [10] developed a model using the index function to track the interface of multi-phase flow. Although the LBM is a promising method for multi-component/phase flows, one of disadvantages is that all the schemes listed above are limited to small density ratio (less than 20) due to numerical instability. Obviously, this is not realistic for most two-phase systems e.g. the density ratio of liquid–gas systems is usually larger than 100, and even the density ratio of water to air is about 1000. To overcome this difficulty, Inamuro et al. [1] proposed a LBM for incompressible two-phase flows with large density differences by using the projection method. In this method, two particle velocity distribution functions are used. One is used for calculating the order parameter to track the interface between two different fluids; the other is for calculating the predicted velocity field without pressure gradient. The corrected velocity satisfying the continuity equation can be obtained by solving a Poisson equation.

As we all know that, when a liquid–gas interface meets a solid surface, capillary forces drive it towards equilibrium. A finite steady-state contact angle, known as partial wetting, can be reached due to the balance of surface tension forces. There is a large class of industrial processes which involve motions of multi-phase fluids on a partial wetting surface. The operations ranging from painting, coating, inkjet printing to lubrication and gluing are a few examples. Therefore, Briant et al. [2–4] developed an approach based on the free-energy LBM model introduced by Swift et al. [8,9] to simulate partial wetting and contact line motion in single or two-component, two-phase fluids. Unfortunately, this method naturally inherits the disadvantage of the original free-energy LBM model of Swift et al. and can only be used to simulate two-phase problems with a small density ratio. The maximum density ratio in the simulations of droplets on partial wetting surfaces [11–13] was reported just around 2.

Obviously, in order to simulate a flow of two-phase fluids with a large density ratio on a partial wetting wall, a new scheme of the LBM is needed. The aim of this paper is to develop such type of scheme combining the advantages of both methods developed by Inamuro et al. [1] and Briant et al. [2–4] to simulate the complex two-phase flow on partial wetting surface. In the present study, the dynamics of liquid drops on uniform and heterogeneous wetting walls is simulated numerically by the proposed method. The results of simulation are compared with those of theoretical predictions.

2. New scheme of the lattice Boltzmann method

A new scheme of the lattice Boltzmann method for simulating two-phase fluid with a large density ratio and meanwhile dealing with the interaction between fluid–fluid interface and a partial wetting wall is proposed and described below.

2.1. Two-phase lattice Boltzmann model

For a three-dimensional 15-velocity (D3Q15) LBM model, as shown in Fig. 1, the particle velocity, $\mathbf{e}_\alpha$ ($\alpha = 0, 1, \ldots, 14$), is given by

$$[\mathbf{e}_0, \mathbf{e}_1, \mathbf{e}_2, \mathbf{e}_3, \mathbf{e}_4, \mathbf{e}_5, \mathbf{e}_6, \mathbf{e}_7, \mathbf{e}_8, \mathbf{e}_9, \mathbf{e}_{10}, \mathbf{e}_{11}, \mathbf{e}_{12}, \mathbf{e}_{13}, \mathbf{e}_{14}] = \begin{bmatrix} 0 & 1 & 0 & 0 & -1 & 0 & 0 & 1 & -1 & 1 & 1 & -1 & 1 & -1 & -1 \\ 0 & 0 & 1 & 0 & 0 & -1 & 0 & 1 & 1 & -1 & 1 & -1 & -1 & 1 & -1 \\ 0 & 0 & 0 & 1 & 0 & 0 & -1 & 1 & 1 & 1 & -1 & -1 & -1 & -1 & 1 \end{bmatrix}. \quad (1)$$

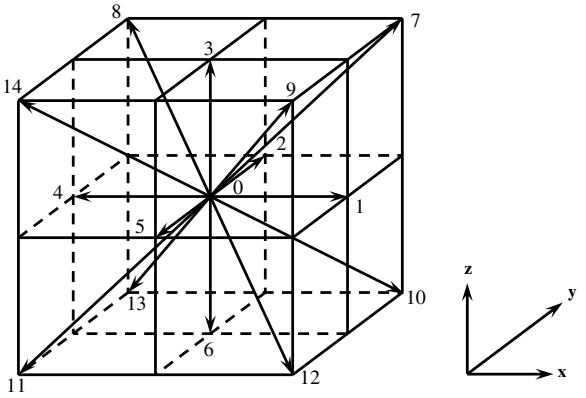

Fig. 1. Discrete velocity set of three-dimensional 15-velocity (D3Q15) model.

To simulate a two-phase fluid flow, two particle velocity distribution functions, f_α and g_α, are introduced. Function f_α is used to calculate the order parameter, ϕ, which distinguishes the two phases. Function g_α is used to calculate the predicted velocity, $\mathbf{u}^*$, of the two-phase fluids without a pressure gradient. The evolution of the particle distribution functions $f_\alpha(\mathbf{x},t)$ and $g_\alpha(\mathbf{x},t)$ with particle velocity $\mathbf{e}_\alpha$ at the point $\mathbf{x}$ and time t is calculated by the following equations:

$$f_\alpha(\mathbf{x}+\mathbf{e}_\alpha\delta_t, t+\delta_t) = f_\alpha^{(\mathrm{eq})}(\mathbf{x},t), \tag{2}$$

$$g_\alpha(\mathbf{x}+\mathbf{e}_\alpha\delta_t, t+\delta_t) = g_\alpha^{(\mathrm{eq})}(\mathbf{x},t), \tag{3}$$

where $\delta_t = 1$ is the time step during which the particles travel the lattice spacing; $f_\alpha^{(\mathrm{eq})}$ and $g_\alpha^{(\mathrm{eq})}$ are the corresponding equilibrium states of f_α and g_α, given by

$$f_\alpha^{(\mathrm{eq})}(\mathbf{x},t) = H_\alpha\phi + F_\alpha\left[p_0 - k\phi\nabla^2\phi - \frac{k}{6}|\nabla\phi|^2\right] + 3\omega_\alpha\phi(\mathbf{e}'_\alpha\cdot\mathbf{u}) + \omega_\alpha k\mathbf{e}'_\alpha\cdot\mathbf{G}(\phi)\cdot\mathbf{e}_\alpha, \tag{4}$$

$$\begin{aligned} g_\alpha^{(\mathrm{eq})}(\mathbf{x},t) = {} & \omega_\alpha\left[1 + 3(\mathbf{e}'_\alpha\cdot\mathbf{u}) + \frac{9}{2}(\mathbf{e}'_\alpha\cdot\mathbf{u})^2 - \frac{3}{2}\mathbf{u}^2 + \frac{3}{4}\mathbf{e}'_\alpha\cdot(\nabla\mathbf{u}+\mathbf{u}\nabla)\cdot\mathbf{e}_\alpha\right] \\ & + \omega_\alpha\frac{k}{\rho}\mathbf{e}'_\alpha\cdot\mathbf{G}(\phi)\cdot\mathbf{e}_\alpha - \frac{2}{3}F_\alpha\frac{k}{\rho}|\nabla\phi|^2 + 3\omega_\alpha\frac{1}{\rho}\nabla\cdot[\mu(\nabla\mathbf{u}+\mathbf{u}\nabla)]\cdot\mathbf{e}_\alpha, \end{aligned} \tag{5}$$

where $\mathbf{u}$, ρ and μ are the macroscopic velocity, density and dynamic viscosity, respectively

$$\omega_\alpha = \begin{cases} 2/9, & \alpha = 0, \\ 1/9, & \alpha = 1,\ldots,6, \\ 1/72, & \alpha = 7,\ldots,14, \end{cases} \quad F_\alpha = \begin{cases} -7/3, & \alpha = 0, \\ 1/3, & \alpha = 1,\ldots,6, \\ 1/24, & \alpha = 7,\ldots,14, \end{cases} \quad H_\alpha = \begin{cases} 1, & \alpha = 0, \\ 0, & \alpha = 1,\ldots,14 \end{cases} \tag{6}$$

and

$$\mathbf{G}(\phi) = \frac{9}{2}(\nabla\phi)(\phi\nabla) - \frac{3}{2}|\nabla\phi|^2\mathbf{I}. \tag{7}$$

In the above equations, k is a constant parameter for determining the width of interface and the strength of surface tension; $\mathbf{I}$ is a unit tensor of second-order. Given that $\psi(\phi)$ is the bulk free-energy density, then

$$p_0 = \phi\frac{\partial\psi}{\partial\phi} - \psi. \tag{8}$$

The macroscopic quantities, $\mathbf{u}^*$, ϕ, ρ, μ can be evaluated as

$$\phi = \sum_\alpha f_\alpha, \quad \mathbf{u}^* = \sum_\alpha \mathbf{e}_\alpha g_\alpha, \tag{9}$$

$$\rho = \begin{cases} \rho_G, & \phi < \phi_G, \\ \frac{\phi-\phi_G}{\phi_L-\phi_G}(\rho_L-\rho_G)+\rho_G, & \phi_G \leqslant \phi \leqslant \phi_L, \\ \rho_L, & \phi > \phi_L, \end{cases} \tag{10}$$

$$\mu = \frac{\rho-\rho_G}{\rho_L-\rho_G}(\mu_L-\mu_G)+\mu_G, \tag{11}$$

where ϕ_L and ϕ_G are respectively the maximum and minimum order parameter for marking bulk liquid and gas; ρ_L and ρ_G are respectively the density of liquid and gas phases; μ_L and μ_G are respectively the dynamic viscosity of liquid and gas phases. In Eq. (10), a simple linear function, rather than the sine function used in Inamuro's model [1], of order parameter is applied to approximate the density within the interface; this enables the present method to obtain $f_\alpha^{(eq)}(\mathbf{x},t)$ and $g_\alpha^{(eq)}(\mathbf{x},t)$ in a more simplified form and thereby cost less for computational resource. For example, the calculations of second-order tensor $\mathbf{G}(\rho)$, first partial derivative of ρ, etc., which are necessary in Inamuro's model [1], can be avoided in the present method.

It should be pointed out that the predicted velocity $\mathbf{u}^*$ is not divergence free. To obtain the velocity field which satisfies the continuity equation ($\nabla\cdot\mathbf{u}=0$), $\mathbf{u}^*$ is corrected by following equations:

$$\mathbf{u}-\mathbf{u}^* = -\frac{\nabla p}{\rho}, \tag{12}$$

$$\nabla\cdot\mathbf{u}^* = \nabla\cdot\left(\frac{\nabla p}{\rho}\right), \tag{13}$$

where p is the pressure of the two-phase fluid, which can be obtained by solving Eq. (13) in the following LBM framework:

$$h_\alpha(\mathbf{x}+\mathbf{e}_\alpha, n+1) = h_\alpha(\mathbf{x},n) - \frac{1}{\tau}[h_\alpha(\mathbf{x},n)-\omega_\alpha p(\mathbf{x},n)] - \frac{\omega_\alpha}{3}\frac{1}{\rho}\nabla\cdot\mathbf{u}^*, \tag{14}$$

where n is the number of iterations and $\tau = 0.5 + 1/\rho$ is the relaxation time. The pressure at step $n+1$ is given by

$$p(\mathbf{x},n+1) = \sum_\alpha h_\alpha(\mathbf{x},n+1). \tag{15}$$

The convergent pressure p is determined when

$$\forall\mathbf{x}\in V, \quad |p(\mathbf{x},n+1)-p(\mathbf{x},n+1)| < \varepsilon, \tag{16}$$

where V denotes the whole computational domain. Substituting the newly obtained pressure p into and solving Eq. (12) gives the corrected velocity field $\mathbf{u}$. This method can be used to simulate two-phase flows with the density ratio up to 1000 [1].

2.2. Partial wetting boundary

To implement the wetting boundary condition, here a Landau free-energy function [3,4] is introduced as

$$\Psi = \int_V \mathrm{d}V[\psi(\phi) + k(\nabla\phi)^2/2], \tag{17}$$

where the square of gradient term on the right-hand side of the equation expresses the contribution to the free-energy excess of the interfacial region which defines the surface energy. Obviously, the bulk free-energy density $\psi(\phi)$ should be defined first of all. In this paper, a new form of free energy (rather than the van der Waals free energy used in the traditional free-energy model) is proposed to calculate wall–fluid surface tensions in a closed form. For an isothermal system, assuming the free-energy density $\psi(\phi)$ takes the following simple form particularly as [14]

$$\psi(\phi) = \beta(\phi-\phi_G)^2(\phi-\phi_L)^2 + \mu_b\phi - p_b, \tag{18}$$

where β is the constant relating to interfacial thickness. Differentiation of Eq. (18) yields the chemical potential

$$\mu_c = 4\beta(\phi - \phi_L)(\phi - \phi_G)(\phi - \phi_M) + \mu_b, \tag{19}$$

where $\phi_M = (\phi_L + \phi_G)/2$; μ_b and p_b are the bulk chemical potential and bulk pressure, respectively.

By substitution of Eq. (18), Eq. (8) becomes

$$p_0 = \beta(\phi - \phi_L)(\phi - \phi_G)(3\phi^2 - \phi\phi_L - \phi\phi_G - \phi_L\phi_G) + p_b. \tag{20}$$

Let $\beta = 0.5$, $\phi_G = 0.1$ and $\phi_L = 0.4$, a corresponding $(p_0 - p_b)$–ϕ diagram is obtained as shown in Fig. 2. It can be seen from the figure that there exist four possible solutions of ϕ which satisfy the condition of $p_0 = p_b$. Two of them (points B and D), where $\phi = \phi_L$ and ϕ_G, represent two different phases. The others (points A and C) lie on the unstable portions of the curve where $dp_0/d\phi < 0$. This unstable mechanism forces the fluid into one of its two separate stable states, causing phase segregation.

In a plane interface under an equilibrium condition, the density profile across the interface on equilibrium is represented as

$$\phi(z) = \frac{\phi_L + \phi_G}{2} + \frac{\phi_L - \phi_G}{2}\tanh\left(\frac{2z}{D}\right), \tag{21}$$

where z is the coordinate normal to the interface; the interface thickness D is given by

$$D = \frac{4}{\phi_L - \phi_G}\sqrt{\frac{k}{2\beta}}. \tag{22}$$

The fluid–fluid (liquid–gas) surface tension force σ_{LG} is expressed as [15]

$$\sigma_{LG} = \frac{(\phi_L - \phi_G)^3}{6}\sqrt{2k\beta}. \tag{23}$$

According to the Young's law [16], when a liquid–gas interface meets a partial wetting solid wall, the contact angle, θ_w, measured in the liquid, can be calculated from a balance of surface tension forces at the contact line as

$$\cos\theta_w = \frac{\sigma_{SG} - \sigma_{SL}}{\sigma_{LG}}, \tag{24}$$

where σ_{SG} and σ_{SL} are the solid–gas and solid–liquid surface tension forces, respectively. To calculate the surface tension forces σ_{SG} and σ_{SL} within a mean field framework, Cahn [17] assumed that the fluid–solid interactions are sufficiently short-range such that they contribute a surface integral to the total free energy of the system. Therefore, the total free energy becomes

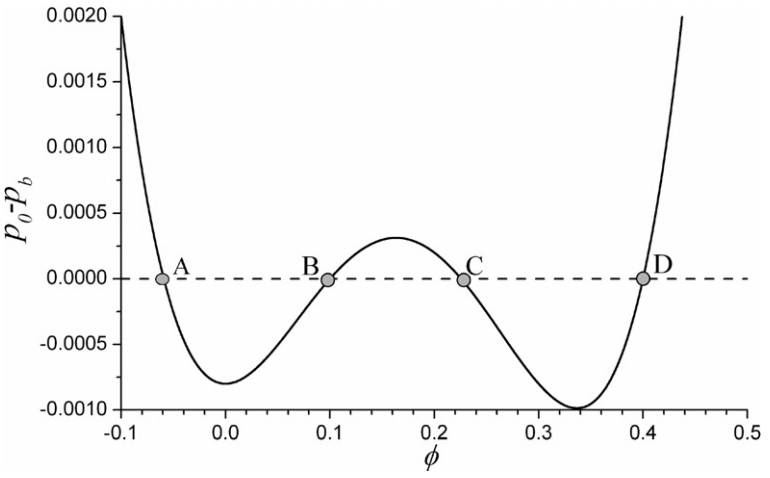

Fig. 2. $(p_0 - p_b)$–ϕ diagram at $\beta = 0.5$, $\phi_G = 0.1$ and $\phi_L = 0.4$.

$$\Psi = \int_V \mathrm{d}V[\psi(\phi) + k(\nabla\phi)^2/2] + \int_s \mathrm{d}S\Phi(\phi_s), \tag{25}$$

where ϕ_s is the order parameter on the wall; S is the surface of volume V.

Now, a one-dimensional problem is considered; where one phase of the non-ideal fluid occupies the region $z > 0$ with a solid wall at $z = 0$. The order parameter far from the wall will be ϕ_L or ϕ_G; while at the wall, $\phi = \phi_s$. Remaining only the first-order term of power series expansion with respect to ϕ_s of $\Phi(\phi_s)$, i.e. $\Phi(\phi_s) = -\lambda\phi_s$, Eq. (25) is reduced to

$$\Psi = \int_V \mathrm{d}z[\psi(\phi) + k(\mathrm{d}\phi/\mathrm{d}z)^2/2] - \lambda\phi_s. \tag{26}$$

Minimizing Eq. (26) by variational calculus subject to natural boundary conditions leads to two conditions as [2]

$$\frac{\partial\psi}{\partial\phi} - k\frac{\mathrm{d}^2\phi}{\mathrm{d}z^2} = \mu_b \quad \text{for } z > 0 \tag{27}$$

and

$$k\left(\frac{\mathrm{d}\phi}{\mathrm{d}z}\right) = \frac{\mathrm{d}\Phi(\phi_s)}{\mathrm{d}\phi_s} = -\lambda \quad \text{for } z = 0. \tag{28}$$

A first integral for Eq. (27) yields

$$\frac{k}{2}\left(\frac{\mathrm{d}\phi}{\mathrm{d}z}\right)^2 = \beta(\phi - \phi_G)^2(\phi - \phi_L)^2 = W(\phi), \tag{29}$$

then ϕ_s can be determined by substituting Eq. (29) into Eq. (28) and be written as

$$-\lambda = \pm\sqrt{2kW(\phi_s)}. \tag{30}$$

Four solutions, $\phi_1 < \phi_2 < \phi_3 < \phi_4$, can be obtained from Eq. (30) if λ is smaller than the height of the double well function defined by $\sqrt{2kW}$ [17]. The corresponding results are

$$\phi_1 = \frac{\phi_L + \phi_G}{2} - \frac{\phi_L - \phi_G}{2}\sqrt{1 + |\Omega|}, \tag{31}$$

$$\phi_2 = \frac{\phi_L + \phi_G}{2} - \frac{\phi_L - \phi_G}{2}\sqrt{1 - |\Omega|}, \tag{32}$$

$$\phi_3 = \frac{\phi_L + \phi_G}{2} + \frac{\phi_L - \phi_G}{2}\sqrt{1 - |\Omega|}, \tag{33}$$

$$\phi_4 = \frac{\phi_L + \phi_G}{2} + \frac{\phi_L - \phi_G}{2}\sqrt{1 + |\Omega|}, \tag{34}$$

where Ω is the wetting potential given by

$$\Omega = \frac{4\lambda}{(\phi_L - \phi_G)^2\sqrt{2k\beta}}. \tag{35}$$

The surface tension between wall and fluid, σ_{SF}, is given by

$$\sigma_{SF} = -\lambda\phi_s + \int \sqrt{2kW}\mathrm{d}\phi. \tag{36}$$

For $\lambda > 0$, the minimized solutions are ϕ_2 if the fluid contacting the wall is a gas and ϕ_4 if the fluid is a liquid. Sequentially, the following expressions for surface tensions are obtained:

$$\sigma_{SG} = -\lambda\phi_2 + \int_{\phi_G}^{\phi_2} \sqrt{2kW}\mathrm{d}\phi = -\lambda\frac{\phi_L + \phi_G}{2} + \frac{\sigma_{LG}}{2} - \frac{\sigma_{LG}}{2}(1 - \Omega)^{3/2}, \tag{37}$$

$$\sigma_{SL} = -\lambda\phi_4 + \int_{\phi_L}^{\phi_4} \sqrt{2kW}\mathrm{d}\phi = -\lambda\frac{\phi_L + \phi_G}{2} + \frac{\sigma_{LG}}{2} - \frac{\sigma_{LG}}{2}(1 + \Omega)^{3/2}. \tag{38}$$

Similarly, the corresponding surface tensions for $\lambda < 0$ are given by

$$\sigma_{SG} = -\lambda\phi_1 + \int_{\phi_1}^{\phi_G} \sqrt{2kW}\,d\phi = -\lambda\frac{\phi_L + \phi_G}{2} + \frac{\sigma_{LG}}{2} - \frac{\sigma_{LG}}{2}(1-\Omega)^{3/2}, \tag{39}$$

$$\sigma_{SL} = -\lambda\phi_3 + \int_{\phi_3}^{\phi_L} \sqrt{2kW}\,d\phi = -\lambda\frac{\phi_L + \phi_G}{2} + \frac{\sigma_{LG}}{2} - \frac{\sigma_{LG}}{2}(1+\Omega)^{3/2}. \tag{40}$$

The wetting angle is determined by substituting Eqs. (23), (37)–(40) into Eq. (24) and written as

$$\cos\theta_w = \frac{(1+\Omega)^{3/2} - (1-\Omega)^{3/2}}{2}. \tag{41}$$

For a given wetting angle in the range of $0 < \theta_w < \pi$, Ω can be obtained from Eq. (41) as

$$\Omega = 2\,\mathrm{sgn}\left(\frac{\pi}{2} - \theta_w\right)\left\{\cos\left(\frac{\gamma}{3}\right)\left[1 - \cos\left(\frac{\gamma}{3}\right)\right]\right\}^{1/2}, \tag{42}$$

where $\gamma = \arccos(\sin^2\theta_w)$ and $\mathrm{sgn}(\xi)$ gives the sign of ξ. It is noted from Eq. (42) that the required wetting potential Ω can be obtained by choosing a desired contact angle θ_w and then calculating λ by solving Eq. (35) with the newly obtained Ω.

Since Eq. (28) is at an equilibrium condition, it is appropriate to be imposed through the equilibrium distribution functions $f_\alpha^{(eq)}$ and $g_\alpha^{(eq)}$. Therefore, in order to introduce a partial wetting wall into the LBM simulation, the following boundary conditions should be imposed on the lattices sites which represent the wall to close Eqs. (4) and (5):

$$\left.\frac{\partial\phi}{\partial z}\right|_{z=0} = -\frac{\lambda}{k}, \tag{43}$$

$$\left.\frac{\partial^2\phi}{\partial z^2}\right|_{z=0} \approx \frac{1}{2}\left(-3\left.\frac{\partial\phi}{\partial z}\right|_{z=0} + 4\left.\frac{\partial\phi}{\partial z}\right|_{z=1} - \left.\frac{\partial\phi}{\partial z}\right|_{z=2}\right), \tag{44}$$

where z is the direction perpendicular to the wall. In this scheme, Eq. (43) is used to determine the first term on the right-hand side of Eq. (44). The second term is calculated by a standard centred finite-difference formula. Finally, Briant et al. [2] have found empirically that the best choice for the third term is a left-handed finite-difference formula taken back into the wall, namely

$$\left.\frac{\partial\phi}{\partial z}\right|_{z=2} \approx \frac{1}{2}(3\phi|_{z=2} - 4\phi|_{z=1} + \phi|_{z=0}). \tag{45}$$

3. Results and discussion

The motion of water droplets at normal temperature surrounded by air on a partial wetting wall is considered. The gravitational force is taken into account by adding the term $-3\omega_\alpha e_{\alpha 3}(1 - \rho_G/\rho)g$ to the right-hand side of Eq. (3), where g is the dimensionless gravitational acceleration. Naturally, the densities of two fluids are set at $\tilde{\rho}_L = 1\times10^3$ kg m^{-3} and $\tilde{\rho}_G = 1.29$ kg m^{-3} (density ratio is about 775), meanwhile the dynamic viscosities of them are at $\tilde{\mu}_L = 1\times10^{-3}$ kg m^{-1} s^{-1} and $\tilde{\mu}_G = 1.935\times10^{-5}$ kg m^{-1} s^{-1}, respectively. The initial surface tension between water and air is of $\tilde{\sigma}_{LG} = 1\times10^{-3}$ kg s^{-2} and the gravitational acceleration is set at $\tilde{g} = 9.8$ m s^{-2}. To relate the physical parameters with simulation parameters, a length scale of $L_0 = 1\times10^{-4}$ m, time scale of $T_0 = 1\times10^{-6}$ s and mass scale of $M_0 = 1\times10^{-12}$ kg are chosen; these lead to the dimensionless parameters: $\rho_L = 1\times10^3$; $\rho_G = 1.29$; $\mu_L = 0.1$; $\mu_G = 1.935\times10^{-3}$; $\phi_L = 0.4$; $\phi_G = 0.1$; $k = 0.05$; and $g = 9.8\times10^{-8}$. Unless otherwise specified, the flowing simulations are within a cuboid computational domain with a no-slip boundary at the lower surface, i.e. the flat partial wetting wall and the free outflow/inflow boundaries at the other five surfaces. ε in Eq. (16) is set as $\varepsilon = 1\times10^{-6}$.

Firstly, the method is applied to the problems of a water droplet spreading on a uniform wetting surface. Initially, as shown in Fig. 3, the shape of droplet is spherical, the distance between the centre of the sphere and the wall is of $r = 1\times10^{-3}$ m; where r is the radius of the initial droplet. The computational domain is filled with air except the location occupied by the water and is divided into $80\times80\times60$ uniform cubic lattices.

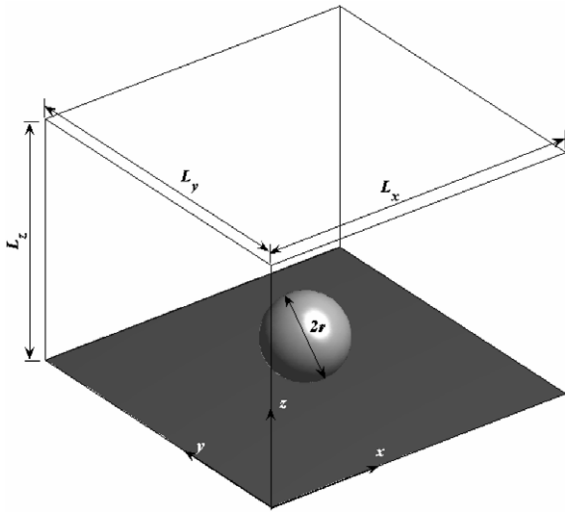

Fig. 3. Computational domain.

In Fig. 4, the droplet is put above a hydrophilic wall. The droplet spreads as time marching, and finally reaches an equilibrium shape; while the contact angle approximates to the initially predicted value, i.e. $\theta_w = \pi/4$. Similar to the conventional CFD method, the numerical instabilities of the LBM for two-phase flows with large density ratios are mainly caused by spurious velocities and/or large oscillations of pressure distribution across the phase interface. The spurious velocities can lead to a violation of the continuity equation, while the larger oscillations of the pressure on the interface may often cause the method to be unstable; thus, the method is, in fact, restricted only to the flow of a smaller density ratio. Therefore, both pressure and velocity distributions across the interface are normally excellent indicators for numerical stability of the LBM method for two-phase flows with large density ratios [18]. In the present method, both velocities and pressures are corrected by solving an additional Poisson equation after each collision-stream step. Thus, such corrections are able to make the velocity field to satisfy the continuity equation and to smooth the pressure distri-

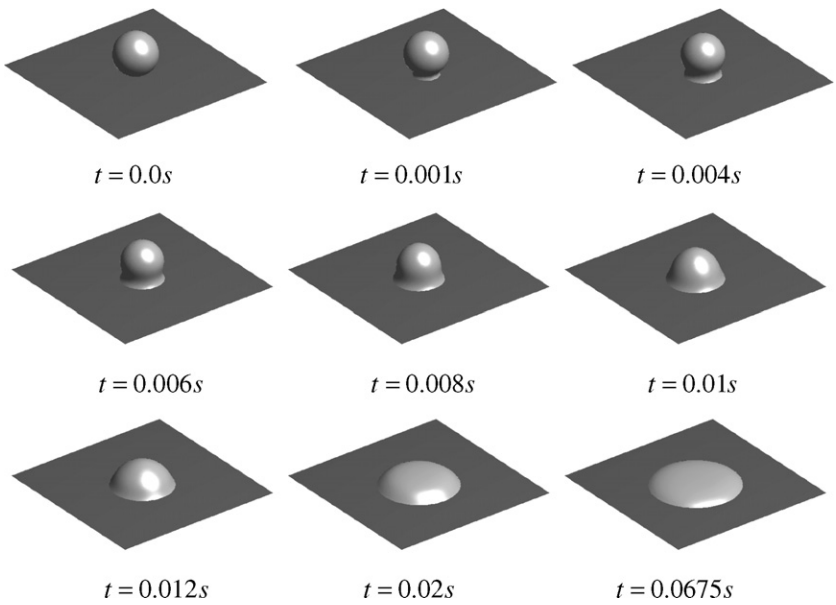

Fig. 4. Snapshots of droplet spreading on a uniform hydrophilic surface, $\theta_w = \pi/4$.

bution across the interface, so that to ensure the numerical stability. In Fig. 5, a velocity field on the cross section of $x = L_x/2$ at $t = 0.006$ s, where the solid line is the interface between two phases, is given to show that the present method can obtain a stable and reasonable velocity distribution.

Fig. 6 shows evolutions with time of the droplet on a flat moderate wall. The contacting area increases with time due to the effect of gravity, the droplet finally reaches an equilibrium shape with contact angle $\theta_w = \pi/2$.

Fig. 7 shows the equilibrium interfacial shapes at $x = L_x/2$ under initial conditions of $\theta_w = \pi/4$ and $\theta_w = \pi/2$, respectively. By measuring the obtained equilibrium contact angles, it is noted that the results of the simulation agree well with those of initial prediction, i.e. $\theta_w = \pi/4$ for the dashed line interface and $\theta_w = \pi/2$ for

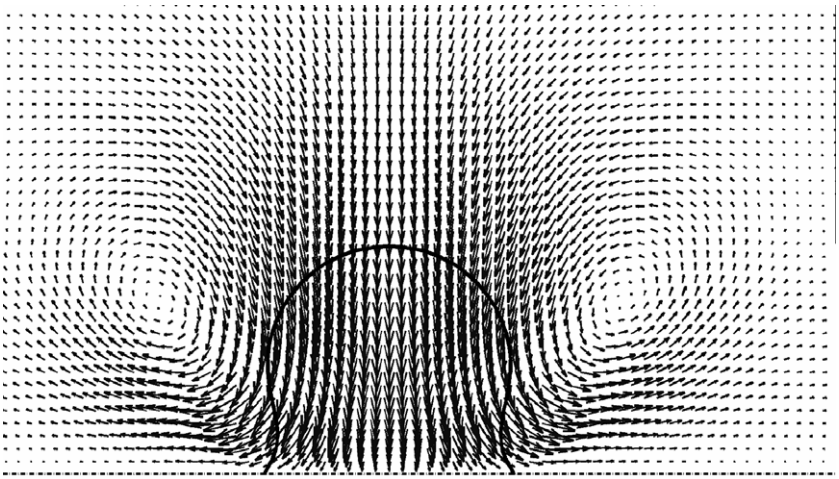

Fig. 5. Velocity distribution on the cross section of $x = L_x/2$, $\theta_w = \pi/4$, $t = 0.006$ s.

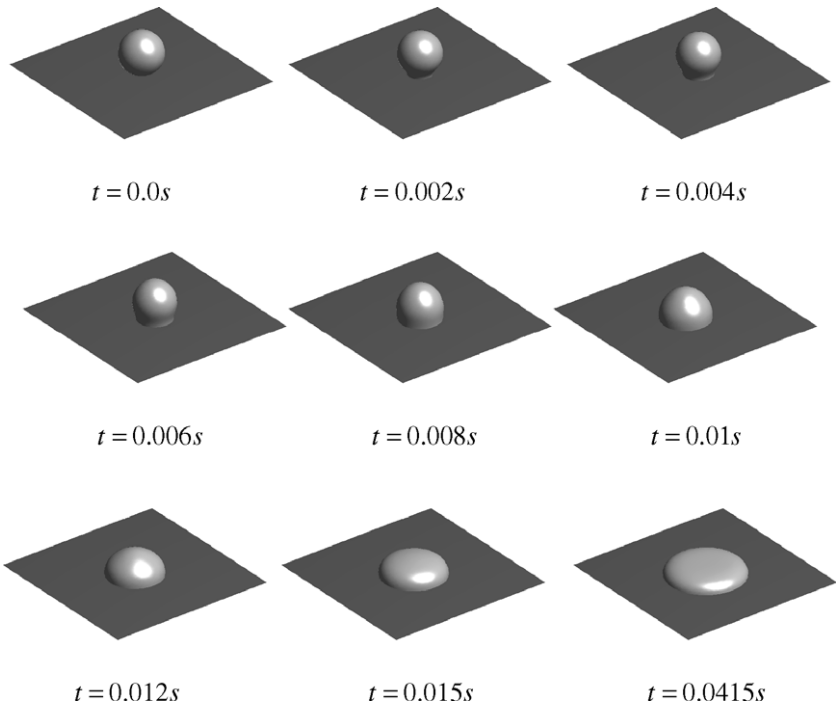

Fig. 6. Snapshots of a droplet spreading on a uniform moderate surface, $\theta_w = \pi/2$.

the solid line interface. This indicates that the present LBM can be used as a reliable way to study fluidic control of wetting related subjects.

Fig. 8 shows how a small hemispherical water droplet evolves with time on a heterogeneous surface. A narrow hydrophobic strip with width of $l = 6 \times 10^{-4}$ m is located at the centreline of the surface where $\theta_w = 5\pi/6$, and the other areas are occupied by the hydrophilic surface with $\theta_w = \pi/6$. The initial droplet which has a radius $r = 1.5 \times 10^{-3}$ m is set at the centre of the wetting surface. As shown in Fig. 8, the droplet stretches over the area occupied by the hydrophilic surface in the early stages of flow evolution due to the adhesive force of the surface. At the same time, the droplet rapidly contracts inward along the hydrophobic strip. With the development of time, the droplet spreads further on the hydrophilic area, and meanwhile contracts inward along the hydrophobic strip and finally breaks up into two smaller droplets. The newly formed droplets continue spreading until an equilibrium state is reached. For a uniform hydrophilic surface separated by a hydrophobic strip, the spreading dynamics of the droplet is affected by three parameters, namely, the width of the

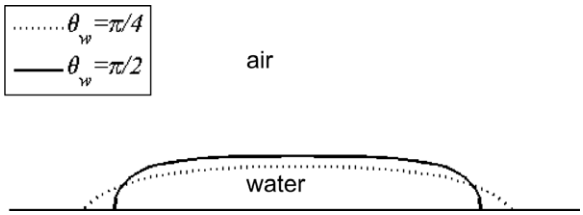

Fig. 7. Equilibrium interfacial shapes at $x = L_x/2$.

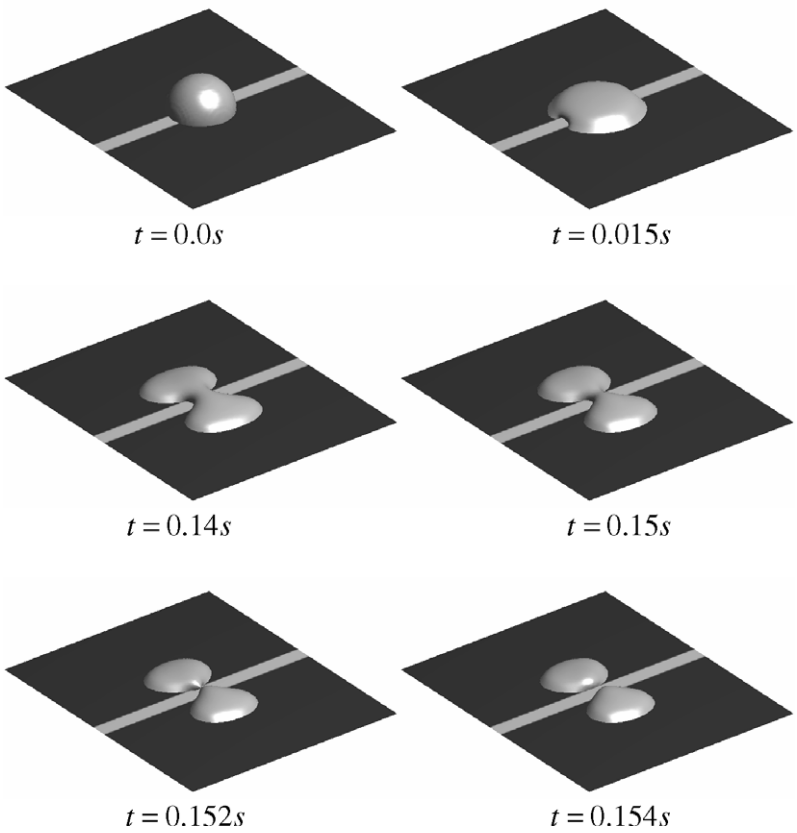

Fig. 8. Snapshots of a droplet spreading on a heterogeneous surface with a hydrophobic strip.

hydrophobic strip, the gravity and the wetting property of the hydrophilic surface [19]. A further examination and analysis of the effects of these three parameters on spreading and break-up of the droplet will be conducted in the near future.

Finally, a single droplet spreading on a heterogeneous surface with intersecting hydrophobic strips is simulated. As shown in Fig. 9, two cross hydrophobic strips ($\theta_w = 5\pi/9$) with width of $l = 9 \times 10^{-4}$ m are located

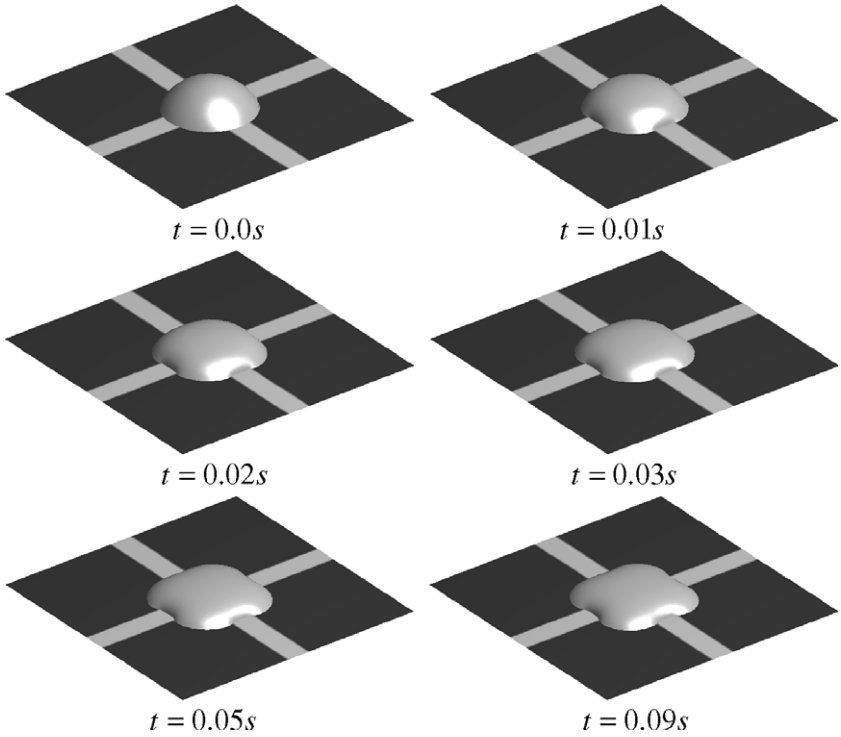

Fig. 9. Snapshots of a droplet spreading on a heterogeneous surface with intersecting hydrophobic strips.

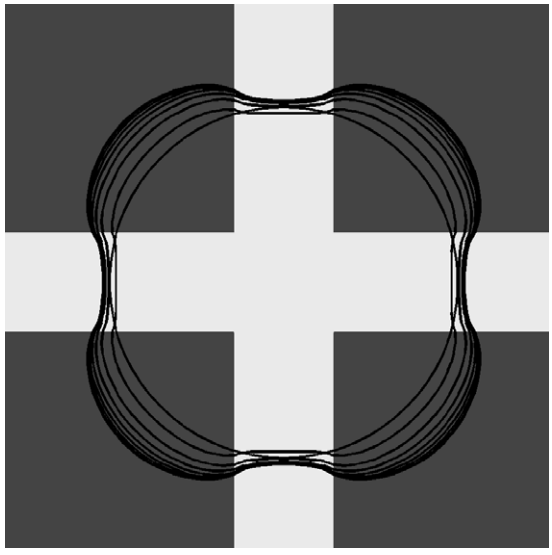

Fig. 10. Contact line for $t = 0$–0.09 s with a 0.01 s interval.

at the centreline of the square surface, the other areas are occupied by the hydrophilic surface with $\theta_w = \pi/4$. Initially, the droplet has a shape of spherical cap with radius of $r = 2 \times 10^{-3}$ m and height of $h = 1 \times 10^{-3}$ m, and is set at the centre of the surface. The shape evolution of the droplet with time is shown in Fig. 9. From the figure, it can be seen that the droplet symmetrically spreads into four hydrophilic sections with the development of time and finally reaches a equilibrium state with a shape of four-leaved flower. Fig. 10 shows the corresponding contact line when t increases from 0 to 0.09 s with an interval of 0.01 s. It is noted by examining the contact lines at $t = 0$ and 0.01 s, respectively, that the droplet experiences a process of contracting inward along the hydrophobic strips at early stage of the evolution.

4. Conclusions

In this paper, a new numerical scheme of the lattice Boltzmann method for calculating liquid droplet behaviour on particle wetting surfaces typically for the system of liquid–gas of a large density ratio has been developed. The method combines the existing models of Inamuro et al. [1] and Briant et al. [2–4] and has developed a novel treatment for partial wetting boundaries which existing when a liquid droplet spreads on a partial wetting surface. In the present study, a water droplet in air (density ratio of 775) spreading on three types of partial wetting surface are studied and simulated based on the current LBM scheme. One is the liquid droplet spreading on a wetting surface with uniform contact angle. The other is a droplet spreading on a heterogeneous wetting wall which combines a uniform hydrophilic surface of low contact angle with a hydrophobic strip of high contact angle; the third case is concerned with a droplet spreading on a wetting surface combined with cross hydrophobic strips. The interactions between the fluid–fluid interface and the partial wetting wall are typically considered in the simulations. The obtained equilibrium contact angles of a droplet spreading on uniform surfaces agree well with those of initial settings. Furthermore, the phenomena of a droplet spreading and breaking up into smaller droplets on a heterogeneous wetting surface have been successfully simulated. These indicate that the present LBM can be used as a reliable way to study fluidic control on heterogeneous surfaces and other wetting related subjects. The current paper mainly focuses on describing the numerical method and case studies; the physical factors influencing droplets spreading and break-up on heterogeneous surfaces and accurate experimental validations will be carried out in the near future.

Acknowledgment

This work is supported by the UK EPSRC (Engineering Physical Science Research Council) under grant EP/D500125/1.

References

[1] T. Inamuro, T. Ogata, S. Tajima, N. Konishi, A lattice Boltzmann method for incompressible two-phase flows with large density differences, J. Comput. Phys. 198 (2004) 628–644.
[2] A.J. Briant, P. Papatzacos, J.M. Yeomans, Lattice Boltzmann simulations of contact line motion in a liquid–gas system, Philos. Trans. Roy. Soc. London A 360 (2002) 485–495.
[3] A.J. Briant, A.J. Wagner, J.M. Yeomans, Lattice Boltzmann simulations of contact line motion: I. Liquid–gas systems, Phys. Rev. E 69 (2004) 031602.
[4] A.J. Briant, J.M. Yeomans, Lattice Boltzmann simulations of contact line motion: II. Binary fluids, Phys. Rev. E 69 (2004) 031603.
[5] S. Chen, G.D. Doolen, Lattice Boltzmann method for fluid flows, Ann. Rev. Fluid Mech. 30 (1998) 329–364.
[6] A.K. Gunstensen, D.H. Rothman, S. Zaleski, G. Zanetti, Lattice Boltzmann model of immiscible fluids, Phys. Rev. A 43 (1991) 4320–4327.
[7] X.W. Shan, H.D. Chen, Lattice Boltzmann model for simulating flows with multiple phases and components, Phys. Rev. E 47 (1993) 1815–1819.
[8] M.R. Swift, W.R. Osborn, J.M. Yeomans, Lattice Boltzmann simulation of nonideal fluids, Phys. Rev. Lett. 75 (1995) 830–833.
[9] M.R. Swift, E. Orlandini, W.R. Osborn, J.M. Yeomans, Lattice Boltzmann simulations of liquid–gas and binary fluid systems, Phys. Rev. E 54 (1996) 5041–5052.
[10] X.Y. He, S.Y. Chen, R.Y. Zhang, A lattice Boltzmann scheme for incompressible multiphase flow and its application in simulation of Rayleigh–Taylor instability, J. Comput. Phys. 152 (1999) 642–663.
[11] A. Dupuis, J.M. Yeomans, Lattice Boltzmann modelling of droplets on chemically heterogeneous surfaces, Future Gener. Comput. Syst. 20 (2004) 993–1001.

[12] A. Dupuis, J.M. Yeomans, Modeling droplets on superhydrophobic surfaces: equilibrium states and transitions, Langmuir 21 (2005) 2624–2629.
[13] H. Kusumaatmaja, A. Dupuis, J.M. Yeomans, Lattice Boltzmann simulations of drop dynamics, Math. Comput. Simul. 72 (2006) 160–164.
[14] D. Jamet, O. Lebaigue, N. Coutris, J.M. Delhaye, The second gradient theory: a tool for the direct numerical simulation of liquid–vapor flows with phase-change, Nucl. Eng. Des. 204 (2001) 155–166.
[15] J.S. Rowlinson, B. Widom, Molecular Theory of Capillarity, Clarendon, Oxford, 1989.
[16] T. Young, An essay on the cohesion of fluids, Philos. Trans. Roy. Soc. London 95 (1805) 65–87.
[17] J.W. Cahn, Critical-point wetting, J. Chem. Phys. 66 (1977) 3667–3672.
[18] T. Lee, C.L. Lin, A stable discretization of the lattice Boltzmann equation for simulation of incompressible two-phase flows at high density ratio, J. Comput. Phys. 206 (2005) 16–47.
[19] Q.M. Chang, J.I.D. Alexander, Analysis of single droplet dynamics on striped surface domains using a lattice Boltzmann method, Microfluid. Nanofluid. 2 (2006) 309–326.